Brillouin zone spin filtering mechanism of enhanced tunneling magnetoresistance and correlation effects in a Co(0001)/*h* -BN/Co(0001) magnetic tunnel junction

Sergey V. Faleev,[1,*] Stuart S. P. Parkin,[1] and Oleg N. Mryasov[2]
[1]*IBM Almaden Research Center, 650 Harry Road, San Jose, California 95120, USA*
[2]*Physics and Astronomy, University of Alabama, Tuscaloosa, Alabama 35487, USA*
(Received 25 August 2014; published 10 December 2015)

The Brillouin zone spin filtering mechanism of enhanced tunneling magnetoresistance (TMR) is described for magnetic tunnel junctions (MTJs) and studied for an example of the MTJ with hcp Co electrodes and hexagonal BN (*h*-BN) spacer. Our calculations based on the local density approximation of density-functional theory (LDA-DFT) for Co(0001)/*h*-BN/Co(0001) MTJ predict high TMR in this device due to Brillouin zone filtering mechanism. Owning to the specific complex band structure of the *h*-BN the spin-dependent tunneling conductance of the system is ultrasensitive to small variations of the Fermi energy position inside the BN band gap. Doping of the BN and, consequentially, changing the Fermi energy position could lead to variation of the TMR by several orders of magnitude. We show also that taking into account correlation effects on beyond DFT level is required to accurately describe position of the Fermi level and thus transport properties of the system. Our study suggests that new MTJ based on hcp Co-Pt or Co-Pd disordered alloy electrodes and *p*-doped hexagonal BN spacer is a promising candidate for the spin-transfer torque magnetoresistive random-access memory.

DOI: 10.1103/PhysRevB.92.235118 PACS number(s): 85.75.−d, 73.40.Rw

I. INTRODUCTION

Theoretical prediction of high TMR in Fe/MgO/Fe MTJ due to so-called symmetry spin filtering mechanism [1,2] and its quick experimental verification [3,4] revolutionized the hard disk drive (HDD) industry during the last decade. On the other hand, continued progress in new areas of magnetic memory technology [for example, spin-transfer torque magnetoresistive random-access memory (STT-MRAM) or spin torque oscillators (STOs)] demands a development of novel MTJ in which a high value of the volume-type magnetocrystalline anisotropy (MCA) of electrodes is as important as high TMR. Nowadays standard Fe-based electrodes have low-volume MCA due to high (cubic) symmetry and thus have to rely on interface anisotropy, which cannot fully satisfy the strict demands of new technology.

In the present paper we consider different mechanism of high TMR in magnetic tunnel junctions, which we call the Brillouin zone spin filtering, and investigate this mechanism in detail for one specific example of low-symmetry (hexagonal) hcp-Co/*h*-BN/hcp-Co junction. We define the Brillouin zone spin filtering (BZ filtering) as a general mechanism of enhanced magnetoresistance in an electrode/spacer/electrode device where spin filtering is provided by (i) existence of the so-called hot spot – a special part in the in-plane two-dimensional surface Brillouin zone (2D SBZ) where the spacer has very high probability of transmission, (ii) absence of states with in-plane wave vector $k_{||}$ corresponding to the hot spot in one spin channel of the magnetic electrode, and (iii) presence of states with corresponding $k_{||}$ in another spin channel of the electrode (see Fig. 1 for illustration).

For illustration of the strength of the BZ filtering effect in MTJ devices let us consider general case when in the hot spot of the spacer the smallest attenuation constant is γ_1, so the eigenstates coming from the electrode with spin channel that has states with $k_{||}$ corresponding to the hot spot will decay as $\exp(-\gamma_1 N)$ inside the spacer, where N is the number of layers of the spacer. On the other hand, the eigenstates of another spin channel that do not have states with $k_{||}$ corresponding to the hot spot will decay much faster, as $\exp(-\gamma_2 N)$, where $\gamma_2 > \gamma_1$ is the smallest attenuation constant available for these states (outside of the hot spot area). Thus, in this example, the BZ filtering mechanism leads to exponential increase of the TMR with N, $TMR \propto \exp[2(\gamma_2 - \gamma_1)N]$. This is a much more pronounced thickness dependence compared to linear or quadratic increase of the TMR with N [5] originated from the symmetry spin filtering where the filtering mechanism works only in close vicinity of some high-symmetry points of 2D SBZ (e.g., Γ point in conventional Fe/MgO/Fe MTJs [1,2]).

In this paper we show that the BZ filtering conditions can be satisfied in *p*-doped BN MTJ with hcp Co electrodes. Realization of the BZ filtering conditions for the low crystal symmetry system such as Co/BN/Co MTJ where high TMR and perpendicular magnetic anisotropy (PMA) could be simultaneously achieved is of significant potential technological interest in the context of novel STT-MRAM technology that has a potential to become a universal memory [6] combining all the strengths and none of the weaknesses of existing memory types.

In STT-MRAM devices the perpendicular magnetic anisotropy (PMA) of electrodes is the preferable option as compared to electrodes with in-plane anisotropy due to faster switching with low current, higher thermal stability, and scalability [7,8]. The requirements on PMA electrodes include high thermal stability at reduced dimensions, low switching current, and high TMR all at the same time. Various PMA materials have been studied for STT-MRAM electrodes, including (Co, Fe)/(Pt, Pd) multilayers [7–9], $L1_0$-ordered (Co, Fe) Pt alloys [10–12], rare-earth/transitional-metal (RE/TM) alloys [13,14], ultrathin CoFeB [15] and CoFeAl [16,17] films, and tetragonal manganese alloys such as Mn_3Ga [18]. Despite intensive research, none of these materials satisfy strict requirements that would allow STT-MRAM to replace conventional memory

*svfaleev@us.ibm.com

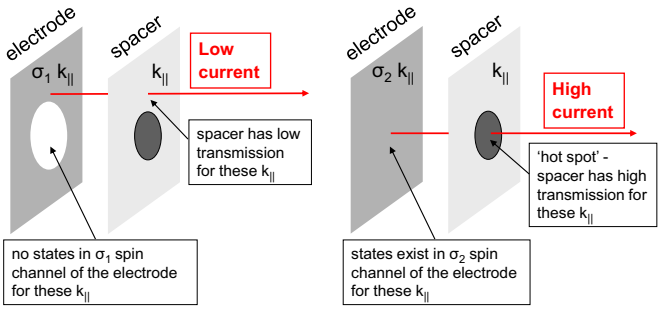

FIG. 1. (Color online) Illustration of the Brillouin zone spin filtering mechanism of enhanced TMR. In application to the Co/BN/Co MTJ the Brillouin zone spin filtering conditions illustrated on this figure occur if Co Fermi energy is aligned inside the BN band gap close to the valence band maximum of BN. In such case the hot spot is the area near the K point in the surface Brillouin zone – for $k_{||}$ near the K point the BN has very high transmission, while, as shown on Fig. 4(a), Co does not have majority electron states at these $k_{||}$ (see text for details).

today. Electrodes with large concentration of heavy Pt or Pd elements (such as multilayers Co/Pt or Co/Pd) have high PMA but also exhibit a relatively large Gilbert damping constant due to strong spin-orbit coupling of Pt and Pd, and, according to the Slonczewski-Berger formula [19,20], high switching current density. PMA in CoFeB/MgO [15] and in Co_2FeAl/MgO MTJs [17] demonstrated recently with ultrathin layers of CoFeB and Co_2FeAl originates from the electrode/spacer interface, not the volume of the electrodes. Finally, TMR in Mn_3Ga/MgO MTJs was found to be very small, far below the application range.

II. BZ FILTERING IN Co/BN/Co MTJ

A. Transmission at zero bias

In the present paper we study the BZ filtering mechanism of (exponentially) large TMR in MTJ based on hcp Co(0001) electrodes and h-BN spacer. h-BN is an ultrahigh chemically stable semiconductor with band gap of ∼6 eV that has a small lattice mismatch with hcp Co. Growth of single and multiple layers of h-BN on Co(0001) has been recently demonstrated [21]. To the best of our knowledge only few studies of Co/BN/Co system exist, mainly with a single sheet of BN spacer [22–24]. The FM/BN/gr/FM(111) MTJ has been suggested in Ref. [25], where used ferromagnet (FM) electrodes fcc Ni and fcc Co do not have PMA. High TMR in this design is achieved due to the BZ filtering mechanism by using graphite (gr) as a spacer that provides spin filtering, while overall resistance of MTJ is regulated by the thickness of the h-BN. In present work we show that complex BN/gr structure is not needed and with optimal realization of the BZ filtering conditions, the h-BN itself can act as a spin filter to produce high TMR. Also, h-BN is more oxidation and intercalation resistant than graphite.

We calculated transmission functions of the Co(0001)/h-BN/Co(0001) MTJ using the equilibrium (zero-bias) Green's function approach within the LDA-based LMTO-ASA formalism [26,27]. The system consists of N_{BN} h-BN sheets sandwiched between two semi-infinite hcp Co electrodes. The in-plane lattice constant, 2.50 Å, and distances between Co layers, 2.03 Å, and between h-BN layers, 3.33 Å, were set to experimental values for bulk hcp Co and h-BN. Positions of surface B and N atoms relative to the surface Co layer were calculated by using VASP molecular dynamic program [28]. In lowest-energy configuration N and B atoms occupy the top and hcp sites with distance between Co and BN layers equal to 3.31 Å (see, e.g., Ref. [23] for definition of top, fcc, and hcp sites on the Co(0001) surface). Two configurations (N,B) = (top, hcp) and (N,B) = (top, fcc) have similar energies, in agreement with previous calculations for a monolayer of h-BN on hcp Co(0001) surface [23,24] and experimental observations [21]. Other possible configurations (N,B) = (hcp, top), (hcp, fcc), (fcc, top), and (fcc, hcp) have slightly higher energy (0.02–0.03 eV per unit cell).

Transmission functions $T_{\uparrow\uparrow}$, $T_{\downarrow\downarrow}$, and $T_{\uparrow\downarrow}$ calculated at zero bias voltage for Co(0001)/h-BN/Co(0001) MTJ with $N_{BN} = 4$, 6, 8, and 10 are shown on Fig. 2. Here $T_{\uparrow\uparrow}$ and $T_{\downarrow\downarrow}$ are transmission in majority and minority channels calculated for parallel magnetization configuration of electrodes and $T_{\uparrow\downarrow}$ is transmission calculated for antiparallel magnetization configuration of electrodes. Corresponding zero-bias TMR defined as $TMR(E) = (T_{\uparrow\uparrow} + T_{\downarrow\downarrow} - 2T_{\uparrow\downarrow})/2T_{\uparrow\downarrow}$ are shown on Fig. 3 for $N_{BN} = 4$, 6, 8, and 10 as function of energy. As seen on Fig. 2 the sharp drop of transmission function $T_{\downarrow\downarrow}$ occurs at the valence band maximum (VBM), $E_V = E_F - 0.2$ eV, of the h-BN slab [Fig. 2(b)], while the sharp drop of $T_{\uparrow\uparrow}$ [Fig. 2(a)] and $T_{\uparrow\downarrow}$ [Fig. 2(c)] occurs at different energy, $E = E_F - 0.6$ eV, which corresponds to the valence band edge of BN states in the part of the SBZ available for majority Co electrons. (As shown on Fig. 4(a), there are no majority Co states in the part of the SBZ near the K point where BN has the VBM, see Fig. 4(c).) The difference in the highest energies of the BN valence states for $k_{||}$ available to the majority and minority Co electrons leads to the exponential increase of the $TMR(E)$ with N in the energy range $E_F - 0.6$ eV $< E < E_F - 0.2$ eV (see Fig. 3).

Let us start discussion of the behavior of the transmission functions shown on Fig. 2 with an explanation of why the drop of the functions at the edge energies ($E_F - 0.2$ eV for $T_{\downarrow\downarrow}$ and $E_F - 0.6$ eV for $T_{\uparrow\uparrow}$ and $T_{\uparrow\downarrow}$) is so sharp – transmission functions change by many orders of magnitude when energy varies on a scale of 0.1 eV near the edge energy.

Figures 4(c) and 5 show the real bands and selected complex bands of bulk h-BN. In bulk h-BN the mode with smallest attenuation constant $\gamma(E) = \mathrm{Im}(k_z)$ (shown by dashed green line in Fig. 5) is the mode with $k_{||} = 0$ for all energies, E, inside the band gap except energies in close vicinity of the valence band maximum, E_V, or conduction band minimum, E_C. As seen on Fig. 5 this evanescent mode continuously connects two real h-BN bands [shown also along A-Γ line on Fig 4(c)]: highly dispersive conduction band with energy $E_V + 4.8$ eV at Γ point and valence band with energy $E_V - 4.1$ eV at Γ point. As seen on Fig. 5 the maximum of this $\gamma(E)$ occurs at $E \sim E_V$. This explains why the transmission functions shown in Fig. 2 have a tendency to smoothly decrease (on logarithmic scale) when energy decreases from E_C to E_V with a minimum near E_V.

The valence band maximum (VBM) of h-BN corresponds to a state with a wave vector near the K point, so for E slightly

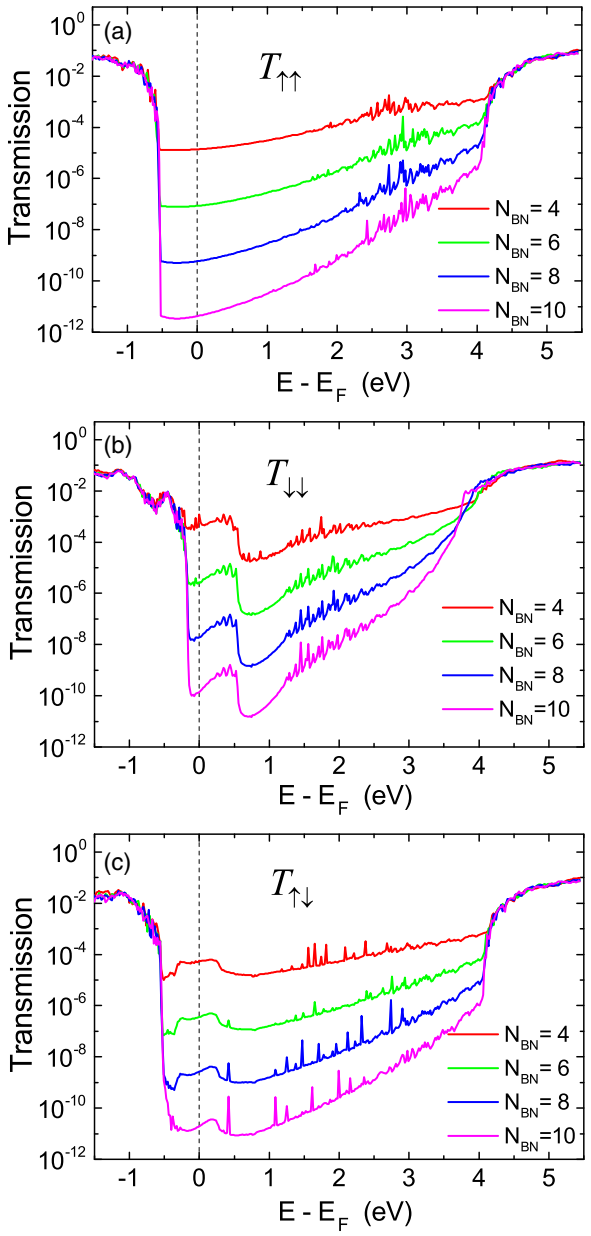

FIG. 2. (Color online) Transmission functions (a) $T_{\uparrow\uparrow}$, (b) $T_{\downarrow\downarrow}$, and (c) $T_{\uparrow\downarrow}$ calculated at zero voltage for Co(0001)/h-BN/Co(0001) MTJ with $N_{BN} = 4$, 6, 8, and 10.

above E_V the evanescent mode with smallest attenuation constant changes and becomes the mode with $k_{||}$ close to the K point (shown by dashed red line on Fig. 5). Since the valence band along the H-K line with energy near E_V is almost flat [see Fig. 4(c) and solid red line on Fig. 5], the corresponding $\gamma(E)$ increases very fast when E increases above E_V, which explains the sharp drop of the transmission functions at energies slightly above the VBM, E_V.

Thus, specific features of the complex band structure of BN described above are responsible for ultrasensitivity of the TMR of Co/BN/Co MTJ to small changes of energy near the VBM (in other words, to the position of the Fermi energy inside the BN band gap.) We note that transmission functions of conventional MgO-based Fe/MgO/Fe MTJs do not exhibit

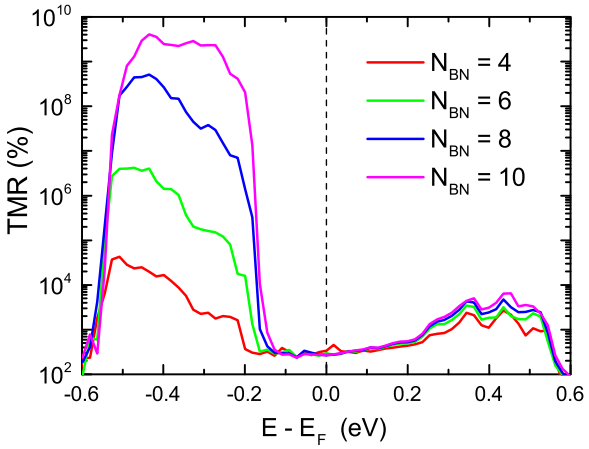

FIG. 3. (Color online) TMR calculated at zero voltage for Co(0001)/h-BN/Co(0001) MTJ with $N_{BN} = 4$, 6, 8, and 10 shown as function of energy.

sharp features as the function of energy near the MgO band gap edges, since MgO has simpler complex band structure as compared to that of h-BN.

Now let us provide more details for the explanation of why the sharp drop of $T_{\uparrow\uparrow}$ and $T_{\downarrow\downarrow}$ shown on Fig. 2 occurs at different energies. The left panels of Fig. 7 show bands of repeated slabs of 9 hcp Co and 5 h-BN layers calculated along symmetry lines of 2D SBZ by the LDA-based FP-LMTO method. Green and blue colors of bands on Fig. 7 are mixed according to the values of the projections of the wave functions to Co and BN atomic orbitals, correspondingly. Figure 7(a) shows that the highest energy at which majority Co states and valence h-BN states coexist at the same $k_{||}$ is $E'_V = E_F - 0.6$ eV. On the other hand Fig. 7(d) shows that the highest energy at which minority Co states and valence h-BN states coexist at the same $k_{||}$ (with $k_{||}$ near the K point) is the VBM of h-BN $E_V = E_F - 0.2$ eV. This explains why the sharp drop of $T_{\downarrow\downarrow}$ and $T_{\uparrow\uparrow}$ (and $T_{\uparrow\downarrow}$) shown on Fig. 2 occur at two different energies: $E_F - 0.2$ eV and $E_F - 0.6$ eV, correspondingly.

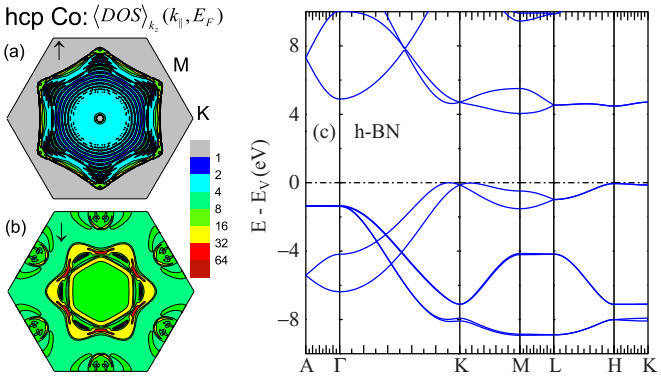

FIG. 4. (Color online) (a) majority and (b) minority electrons DOS of bulk hcp Co at E_F averaged over the wave vector along c axis, k_z, shown as function of in-plane $k_{||}$ in 2D surface Brillouin zone (SBZ). Note absence of majority electron states near K and M points (gray color represent $DOS = 0$). (c) bands of bulk h-BN calculated by full potential (FP) LMTO method.

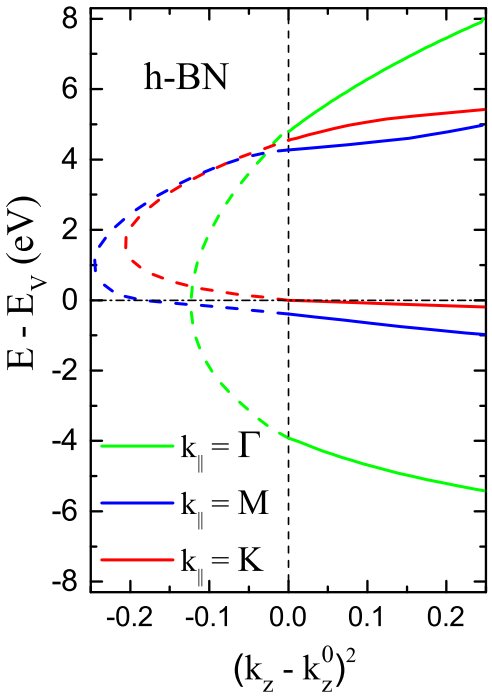

FIG. 5. (Color online) Selected complex bands of h-BN calculated by Green's function approach within the LMTO-ASA framework [26,27] shown at three $k_{||} = \Gamma, M$, and K as function of $(k_z - k_z^0)^2$, where k_z^0 is the wave vector corresponding to the lowest energy of conduction band at given $k_{||}$, $k_z^0 = 0$ for $k_{||} = \Gamma$ and M, and $k_z^0 = 0.5$ for $k_{||} = K$ [$k_z^0 = 0.5$ with $k_{||} = K$ is the H point in the 3D BZ of bulk BN, see Fig. 4(c)]. Positive $(k_z - k_z^0)^2 > 0$ (shown by solid lines) represent real BN states while negative $(k_z - k_z^0)^2 < 0$ (shown by dashed lines) represent evanescent modes, $k_z(E) = k_z^0 + i\gamma(E)$. (The wave vectors k_z are shown in units of $2\pi/c$, where c is the distance between BN sheets.)

Let us stress again that it is the BZ filtering mechanism that is responsible for several orders of magnitude difference of $T_{\downarrow\downarrow}$ transmission compared to $T_{\uparrow\uparrow}$ (and $T_{\uparrow\downarrow}$) at energies in the range ($E_F - 0.2$ eV, $E_F - 0.6$ eV). More specifically, for these energies the real states of BN near the K point provide metallic transmission with zero attenuation constant $\gamma_1 = 0$ for minority Co electrons (in other words, the hot spot near the K point exists for minority Co electrons). On the other hand, there are no majority Co states in vicinity of K point at these energies. The eigenstates of majority Co electrons with $k_{||}$ in other parts of the SBZ exponentially decay with nonzero attenuation constant $\gamma_2 > 0$. As a result, TMR increases exponentially, $TMR(E) \propto \exp(2N\gamma_2)$, with increased number of BN layers (see Fig. 3). This is exactly the situation described in our definition of the BZ filtering effect.

B. Transmission and current at finite bias

In order to calculate TMR as a function of applied bias voltage we used the nonequilibrium Green's function (NEGF) LMTO-ASA theory developed recently [29]. The I-V curves of $I_{\uparrow\uparrow}$, $I_{\downarrow\downarrow}$, and $I_{\uparrow\downarrow}$ currents per unit cell area are shown on Fig. 6(a) for $N_{BN} = 6$ and Fig. 6(b) for $N_{BN} = 8$. Corresponding nonequilibrium $TMR(V) = (I_{\uparrow\uparrow} + I_{\downarrow\downarrow} - 2I_{\uparrow\downarrow})/2I_{\uparrow\downarrow}$ is shown on Fig. 6(c) as a function

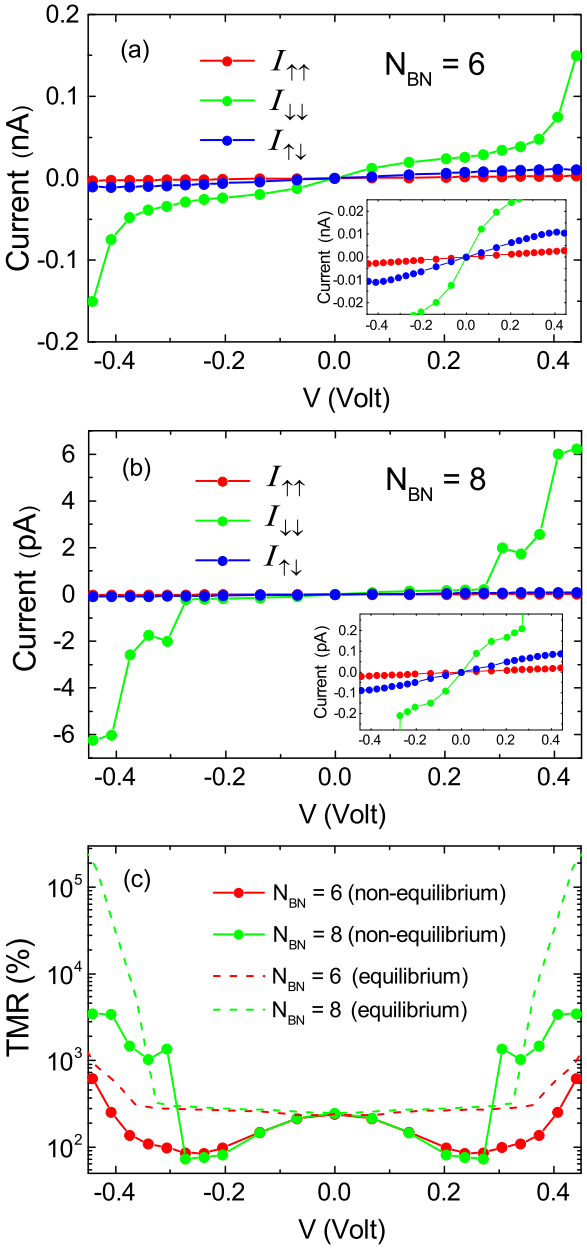

FIG. 6. (Color online) Currents $I_{\uparrow\uparrow}$, $I_{\downarrow\downarrow}$, and $I_{\uparrow\downarrow}$ for (a) $N_{BN} = 6$ and (b) $N_{BN} = 8$, calculated by using nonequilibrium Green's function (NEGF) LMTO-ASA method shown as function of the bias voltage. (c) TMR shown as function of the bias voltage. TMR of nonequilibrium system obtained from the currents presented on Figs. 6(a), 6(b) for $N_{BN} = 6$ (red dots) and $N_{BN} = 8$ (green dots) are compared to equilibrium TMR–TMR obtained by integration the equilibrium transmission functions [shown on Figs. 2(a)–2(c)] over the energy range $(E_F - |e|V/2, E_F + |e|V/2)$ for $N_{BN} = 6$ (red dashed line) and $N_{BN} = 8$ (green dashed line) (see text for details).

of bias voltage for $N_{BN} = 6$ (red dots) and for $N_{BN} = 8$ (green dots). Also we present on Fig. 6(c) the equilibrium TMR–TMR obtained by integration of the equilibrium transmission functions [shown on Figs. 2(a)–2(c)] over the energy range $(E_F - |e|V/2, E_F + |e|V/2)$ for $N_{BN} = 6$ (red dashed line) and $N_{BN} = 8$ (green dashed line). At $V = 0$ the nonequilibrium TMR and equilibrium TMR coincide and is equal to

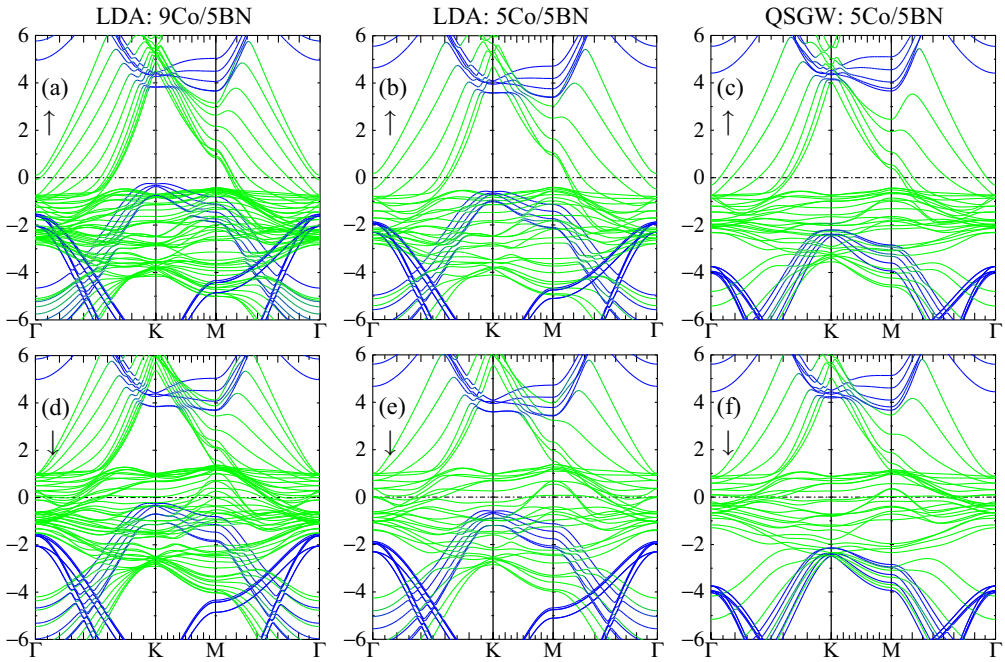

FIG. 7. (Color online) Top panels: majority bands of repeated slabs of (a) 9Co/5BN and (b) 5Co/5BN calculated using the LDA theory, and (c) 5Co/5BN calculated using the QSGW theory (y axis on all graphs is $E - E_F$ in eV). Bottom panels: corresponding minority bands.

$TMR \sim 250\%$ (for both, $N = 6$ and 8). The value of the $TMR \sim 250\%$ at $V = 0$ is mostly due to the fact that the density of states (DOS) of minority electrons of hcp Co at the Fermi energy is significantly larger than the DOS of majority electrons [compare Fig. 4(a) and Fig. 4(b)].

As follows from Fig. 2(b) and Fig. 3 the onset of the sharp drop of the equilibrium transmission $T_{\downarrow\downarrow}$ occurs at $E - E_F \sim -0.17$ eV. Since the energy integration for calculation of the equilibrium TMR is performed over the energy range $(E_F - |e|V/2,\ E_F + |e|V/2)$, the onset of the fast rise of the equilibrium TMR shown on Fig. 6(c) occurs at bias $V = 0.34$ V. Due to the exponential nature of the BZ filtering effect, at $V \sim 0.4$ V the equilibrium TMR for $N = 8$ reaches as much as $10^5\%$. The onset of the rise of the nonequilibrium TMR occurs at similar bias voltages $V \sim 0.3$–0.4 V, but the value of the nonequilibrium TMR is much smaller, $TMR \sim 4000\%$ for $N = 8$ at $V \sim 0.4$ V, due to nonequilibrium effects. Still $TMR \sim 4000\%$ is vary large and possibility of reaching the TMR of such scale is of significant interest for the spintronic device industry.

C. Fermi energy alignment in Co/BN/Co system: LDA vs QSGW

As evident from above discussion large values of TMR are very sensitive to the position of the Fermi energy relative to the VBM of BN, $E_F - E_V$, since onset of high TMR occurs at voltages $V \simeq 2(E_F - E_V)/|e|$, yet V cannot exceed the electrical breakdown limit (operating voltage in typical spintronic device $V < 0.5$ Volt). We studied dependence of $E_F - E_V$ on variations in geometry of the systems by performing FP-LMTO calculations within LDA for repeated slabs of N_{BN} h-BN and N_{Co} hcp Co layers (varying N_{BN} and N_{Co} from 4 to 12) for all configurations of B and N atoms (B, N) = (top, hcp), (top, fcc), (hcp, top), (hcp, fcc), (fcc, top), and (fcc, hcp) and for reasonable variations of positions of surface B, N, and Co atoms. The value of $E_F - E_V$ was found to be stable within LDA/DFT, $E_F - E_V \approx 0.2$ eV, in all above cases for sufficiently thick Co slab with $N_{Co} \geqslant 7$.

On the other hand, it is well known that LDA underestimates band gaps of semiconductors and poorly describes the Schottky barrier heights [30]. To evaluate $E_F - E_V$ on the level beyond LDA we performed calculations for a periodic slab of 5 hcp Co and 5 h-BN layers by using the QSGW theory that is known to describe band gaps and other properties of materials with moderate e-e correlations significantly better than LDA [31–33]. (The restriction to 5Co/5BN slab size was due to heavy computational costs of QSGW.) Figure 7 shows the band structure of majority and minority electrons calculated for periodic 9Co/5BN and 5Co/5BN slabs within the LDA theory, and for 5Co/5BN slabs within the QSGW theory. It is seen that reducing the size of Co slab from 9 layers to 5 layers leads to moderate increase of LDA $E_F - E_V$ from 0.2 eV to 0.5 eV (as mentioned above, $E_F - E_V$ converges to $\approx$0.2 eV for $N_{Co} \geqslant 7$), whereas more accurate inclusion of the e-e correlations within the QSGW theory results in dramatic increase of $E_F - E_V$ to as large as 2.2 eV. Thus, taking into account correlations on beyond LDA level is very important for accurate prediction of the Fermi energy alignment, $E_F - E_V$, at Co/h-BN interface and, consequently, for designing the Co/h-BN/Co MTJ with high TMR.

In order to decrease $E_F - E_V$ from 2.2 eV predicted by QSGW to practical levels $E_F - E_V < 0.1$ eV one can p dope the h-BN (e.g., by Mg). It was recently shown that the Mg acceptor level in Mg-doped h-BN (h-BN:Mg) is as low as 0.031 eV [34], so varying the Mg concentration could bring $E_F - E_V$ to the desired range of $E_F - E_V \leqslant 0.1$ eV. Note that for ideal alignment $E_F - E_V \sim 0$ the TMR could be as high as

several orders of magnitude at very low voltages [to estimate the TMR at small voltage for the case of $E_F - E_V = 0$, one can simply assume that the TMR shown on Fig. 3 has E_F shifted by 0.2 eV to lower energies, so $E_F = E_V$].

III. CONCLUSION

In conclusion, the general Brillouin zone spin filtering mechanism of enhanced TMR is described for magnetic tunnel junctions and studied for an example of MTJ with hcp Co electrodes and h-BN spacer. We suggest new MTJ for STT-MRAM and STO applications based on hcp Co-Pt or Co-Pd disordered alloy electrodes and p-doped h-BN spacer. The PMA of such low-symmetry hcp electrodes originates from the whole volume rather than interfaces and does not require chemical ordering at atomic scale promoting small device-to-device variations, a property important for high yield and low cost. Concentration of heavy Pt or Pd atoms could be balanced between requirements of strong PMA and small damping constant of the alloy (damping constant of pure hcp Co is small, $\alpha_{hcpCo} = 0.004$ [35] at 300K).

Owing to the specific complex band structure of the h-BN the spin-dependent tunneling conductance of the system is ultrasensitive to small variations of the Fermi energy position inside the BN band gap. Our LDA-based NEGF calculations for Co(0001)/h-BN/Co(0001) MTJ show high TMR at $V \geqslant 0.3$ V due to the Brillouin zone filtering mechanism. The critical property needed for high TMR in this MTJ is an alignment of Co E_F very close to VBM of h-BN. LDA predicts $E_F - E_V \approx 0.2$ eV, while $E_F - E_V$ calculated by more accurate QSGW theory increases to 2.2 eV. Thus p doping (e.g., by Mg) of the h-BN is needed to reduce $E_F - E_V$ to a practical range of below 0.1 eV to ensure high TMR (which can be as high as several orders of magnitude) at low voltages. By varying the Mg concentration (and thus $E_F - E_V$) and h-BN slab thickness one can independently regulate the TMR and overall resistance of the MTJ.

ACKNOWLEDGMENTS

S.F. and O.N.M acknowledge the CNMS User support by Oak Ridge National Laboratory Division of Scientific User facilities. O.N.M acknowledges partial support by C-SPIN, one of the six centers of STARnet, a Semiconductor Research Corporation program, sponsored by MARCO and DARPA. S.F. would like to thank Ivan Knez and Barbara Jones for useful discussions, O.N.M. would like to thank Professor J. P. Wang and D. Mazumdar for stimulating discussions.

[1] W. H. Butler, X.-G. Zhang, T. C. Schulthess, and J. M. MacLaren, Phys. Rev. B **63**, 054416 (2001).
[2] J. Mathon and A. Umerski, Phys. Rev. B **63**, 220403(R) (2001).
[3] S. S. P. Parkin, C. Kaiser, A. Panchula, P. M. Rice, B. Hughes, M. Samant, and S.-H. Yang, Nature Mater. **3**, 862 (2004).
[4] S. Yuasa, T. Nagahama, A. Fukushima, Y. Suzuki, and K. Ando, Nature Mater. **3**, 868 (2004).
[5] S. V. Faleev, S. S. P. Parkin, and O. N. Mryasov, arXiv:1511.02577.
[6] Johan Akerman, Science **308**, 508 (2005).
[7] S. Mangin, D. Ravelosona, J. A. Katine, M. J. Carey, B. D. Terris, and Eric E. Fullerton, Nature Mater. **5**, 210 (2006).
[8] H. Meng and J. P. Wang, Appl. Phys. Lett. **88**, 172506 (2006).
[9] K. Mizunuma, S. Ikeda, J. H. Park, H. Yamamoto, H. Gan, K. Miura, H. Hasegawa, J. Hayakawa, F. Matsukura, and H. Ohno, Appl. Phys. Lett. **95**, 232516 (2009).
[10] G. Kim, Y. Sakuraba, M. Oogane, Y. Ando, and T. Miyazaki, Appl. Phys. Lett. **92**, 172502 (2008).
[11] M. Yoshikawa, E. Kitagawa, T. Nagase, T. Daibou, M. Nagamine, K. Nishiyama, T. Kishi, and H. Yoda, IEEE Trans. Magn. **44**, 2573 (2008).
[12] S. Mizukami, S. Iihama, N. Inami, T. Hiratsuka, G. Kim, H. Naganuma, M. Oogane, and Y. Ando, Appl. Phys. Lett. **98**, 052501 (2011).
[13] T. Hatori, H. Ohmori, M. Tada, and S. Nakagawa, IEEE Trans. Magn. **43**, 2331 (2007).
[14] M. Nakayama, T. Kai, N. Shimomura, M. Amano, E. Kitagawa, T. Nagase, M. Yoshikawa, T. Kishi, S. Ikegawa, and H. Yoda, J. Appl. Phys. **103**, 07A710 (2008).
[15] S. Ikeda, K. Miura, H. Yamamoto, K. Mizunuma, H. D. Gan, M. Endo, S. Kanai, J. Hayakawa, F. Matsukura, and H. Ohno, Nature Mater. **9**, 721 (2010).
[16] W. Wang, H. Sukegawa, and K. Inomata, Appl. Phys. Express **3**, 093002 (2010).
[17] Z. Wen, H. Sukegawa, S. Mitani, and K. Inomata, Appl. Phys. Lett. **98**, 242507 (2011).
[18] T. Kubota, Q. Ma, S. Mizukami, X. Zhang, H. Naganuma, M. Oogane, Y. Ando, and T. Miyazaki, Appl. Phys. Express **5**, 043003 (2012).
[19] J. Slonczewski, J. Magn. Magn. Mater. **159**, L1 (1996).
[20] L. Berger, Phys. Rev. B **54**, 9353 (1996).
[21] C. M. Orofeo, S. Suzuki, H. Kageshima, and H. Hibino, Nano Research **6**, 335 (2013).
[22] Oleg V. Yazyev and Alfredo Pasquarello, Phys. Rev. B **80**, 035408 (2009).
[23] Niharika Joshi and Prasenjit Ghosh, Phys. Rev. B **87**, 235440 (2013).
[24] Y. G. Zhou, X. T. Zua, and F. Gaob, Solid State Commun. **151**, 883 (2011).
[25] V. M. Karpan, P. A. Khomyakov, G. Giovannetti, A. A. Starikov, and P. J. Kelly, Phys. Rev. B **84**, 153406 (2011).
[26] I. Turek, V. Drchal, J. Kudrnovsky, M. Sob, and P. Weinberger, *Electronic Structure of Disordered Alloys, Surfaces and Interfaces* (Kluwer, Boston, 1997).
[27] M. van Schilfgaarde, W. R. L. Lambrecht, in *Tight-Binding Approach to Computational Materials Science*, edited by L. Colombo, A. Gonis, and P. Turchi, MRS Symposia Proceedings No. 491 (MRS, Pittsburgh, 1998).
[28] G. Kresse and J. Furthmuller, Phys. Rev. B **54**, 11169 (1996).
[29] S. V. Faleev, F. Leonard, D. A. Stewart, and M. van Schilfgaarde, Phys. Rev. B **71**, 195422 (2005).

[30] G. P. Das, P. Blochl, O. K. Andersen, N. E. Christensen, and O. Gunnarsson, Phys. Rev. Lett. **63**, 1168 (1989).

[31] S. V. Faleev, M. van Schilfgaarde, and T. Kotani, Phys. Rev. Lett. **93**, 126406 (2004).

[32] M. van Schilfgaarde, T. Kotani, and S. V. Faleev, Phys. Rev. Lett. **96**, 226402 (2006).

[33] T. Kotani, M. van Schilfgaarde, and S. V. Faleev, Phys. Rev. B **76**, 165106 (2007).

[34] R. Dahal, J. Li, S. Majety, B. N. Pantha, X. K. Cao, J. Y. Lin, and H. X. Jiang, Appl. Phys. Lett. **98**, 211110 (2011).

[35] S. M. Bhagat and P. Lubitz, Phys. Rev B **10**, 179 (1974).